Harnessing 4f-3d synergy in Ce-Fe heterostructure: a PBA-derived oxygen reservoir for stable high-capacity lithium storage

Shengfa Li,[†a] Jianzhi Wang,[†a] Hang Li,[a] Feng Gao,[b*] Qingyi Lu[a*]

[a] State Key Laboratory of Coordination Chemistry, Coordination Chemistry Institute, Collaborative Innovation Center of Advanced Microstructures, School of Chemistry and Chemical Engineering, Nanjing University, Nanjing 210023, P. R. China. E-mail: qylu@nju.edu.cn

[b] Department of Materials Science and Engineering, Jiangsu Key Laboratory of Artificial Functional Materials, Collaborative Innovation Center of Advanced Microstructures, College of Engineering and Applied Sciences, Nanjing University, Nanjing 210093, P. R. China. E-mail: fgao@nju.edu.cn

[†] These authors contributed equally to this work.

Experimental

Chemicals and materials: Raw chemical materials including cerium nitrate hexahydrate ($Ce(NO_3)_4 \cdot H_2O$, R ≥ 99%), methanol (CH_3OH, R ≥ 99.5%), potassium ferricyanide ($K_3[Fe(CN)_6]$, R ≥ 99.5%) were purchased from Shanghai Hushi Biochemical. All the reagents were used direcly without further purification.

Synthesis of Ce-Fe PBA: In a typical synthetic procedure, 85 mg of cerium nitrate hexahydrate and 45 mg of potassium ferricyanide were dissolved in 2 mL of ultrapure water. Then 8 mL of methanol was injected rapidly into the solution. The mixture was allowed to stand undisturbed for 12 hours. Subsequently, centrifugation was performed to collect the precipitate. The obtained solid was washed with methanol three times and dried at room temperature. Finally, the resulting brown powder was collected.

Synthesis of c-CeO_2/a-$Fe_\alpha O_\beta$: The obtained Ce-Fe PBA was placed in a muffle furnace and annealed at 300 °C.

Synthesis of c-CeO_2/c-Fe_2O_3: The obtained Ce-Fe PBA was placed in a muffle furnace and annealed at 800 °C.

Synthesis of crystalline CeO_2: The c-CeO_2/c-Fe_2O_3 composite was immersed in 2 M HCl solution and heated at 60 °C for 48 hours. The product was then collected by centrifugation, washed, and dried.

Synthesis of Fe-Fe PBA: In a typical synthetic procedure, $K_3[Fe(CN)_6] \cdot 3H_2O$ (1.1 g) and polyvinylpyrrolidone (PVP, K30, MW: ~40000, 38 g) were added to a HCl solution (0.1 M, 500 mL) under magnetic stirring. After stirring for 2 h, a transparent, clear yellow solution was obtained. The solution was then transferred to an electric oven and heated at 80 °C for 24 h. Afterward, the resulting blue product was collected by centrifugation, washed sequentially with ethanol and distilled water (three times each), and finally dried overnight at 35 °C in a vacuum oven.

Synthesis of c-Fe_2O_3: The obtained Fe-Fe PBA was placed in a muffle furnace and annealed at 800 °C.

Characterizations: X-ray diffraction (XRD) patterns were collected on a Bruker D8 ADVANCE diffractometer with Cu Kα radiation. Scanning electron microscopy (SEM) images were obtained on a Hitachi S-4800 scanning electron microscope with an accelerating voltage of 5 kV.

Transmission electron microscope (TEM) images were acquired on JEM-F200 transmission electron microscope with an accelerating voltage of 200 kV. The structure of the sample was tested by Fourier transform infrared spectroscopy (FTIR) with the instrument model of Thermo Scientific Nicolet 380. The specific surface area and pore diameter of the samples were measured by N_2 adsorption/desorption isotherms at 77 K using ASAP 2460 of Mack company. X-ray photoelectron spectroscopy (XPS) (PHI 5000 versa probe type) was used to characterize the chemical environment of the elements in the samples.

Electrochemical measurements

The active materials, few-layer graphene, super P, and polyvinylidene fluoride (PVDF) were mixed at a mass ratio of 6:2:1:1 and ground into a fine, homogeneous powder. Subsequently, an appropriate amount of N-methyl pyrrolidone (NMP) was added to form a slurry, which was then magnetically stirred for 8 hours to ensure thorough dispersion of all components.

The uniformly stirred slurry was evenly coated onto a single-sided smooth copper foil with a thickness of 100 μm. After coating, the copper foil was dried in a vacuum environment at 60 °C for 12 hours to remove the solvent and firmly attach the active materials to the copper foil. Then, the dried copper foil was cut into circular sheets with a diameter of 12 mm, and the mass loading of the active materials on the sheets was approximately 0.35 $mg \cdot cm^{-2}$.

The coin-type cells (CR 2032) were assembled in an argon-filled glove box where the concentrations of oxygen and water were strictly controlled to be less than 1 ppm to avoid unwanted chemical reactions inside the battery. Lithium metal wafers were used as the counter electrode. The electrolyte was a solution of 1.0 M lithium hexafluorophosphate ($LiPF_6$) dissolved in a mixed solvent of ethylene carbonate (EC), dimethyl carbonate (DMC), and ethyl methyl carbonate (EMC) with a volume ratio of 1:1:1. A porous polypropylene separator (PP, Celgard 2400) was employed to separate the positive and negative electrodes.

The battery testing system (Land CT3002A, Wuhan, China) was used to conduct long-term cycling performance tests, rate performance tests, and galvanostatic intermittent titration technique (GITT) tests on the batteries. The test voltage range was set from 0.01 to 3.0 V to evaluate the stability and reversibility of the batteries under different charge-discharge conditions. Cyclic voltammetry (CV) tests were performed using an electrochemical workstation (CHI760D, Chenhua,

Shanghai, China) with a voltage window of 0.01-3.0 V (vs. Li/Li^+) at different scan rates to explore the kinetic processes of the electrode reactions. In addition, electrochemical impedance spectroscopy (EIS) tests were also carried out using the CHI760D electrochemical workstation. An alternating-current signal with an amplitude of 5 mV was applied, and the frequency range was set from 100 kHz to 0.01 Hz to analyze the resistance distribution and electrode process kinetics inside the battery.

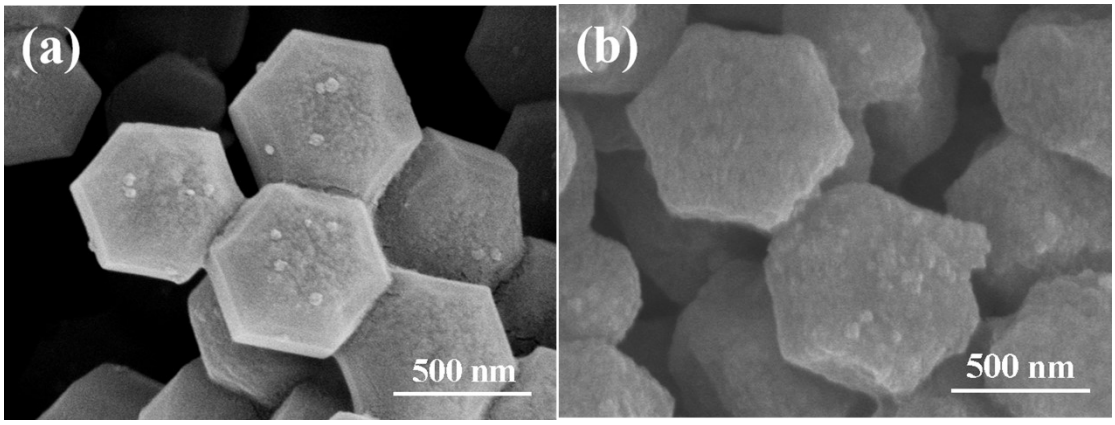

Figure S1 SEM images of (a) Ce-Fe PBA and (b) c-CeO_2/c-Fe_2O_3 (800°C).

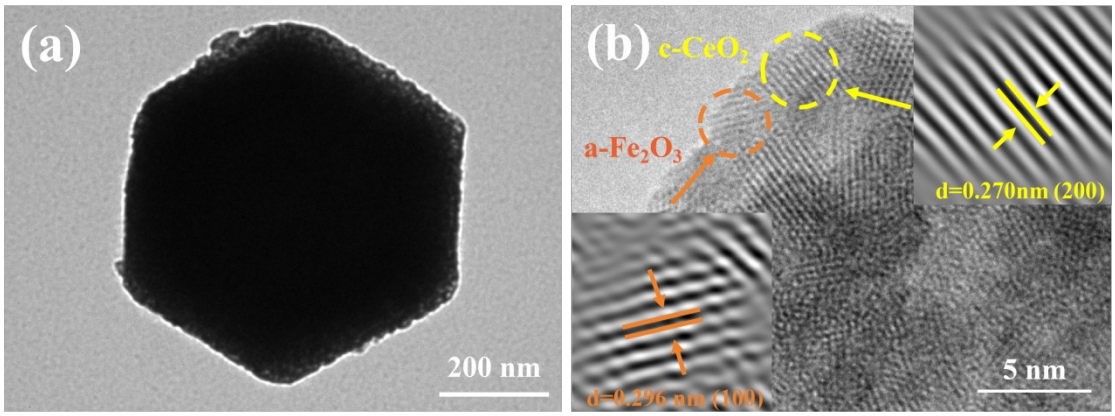

Figure S2 (a) TEM and (b) HRTEM images of c-CeO_2/c-Fe_2O_3 (800°C).

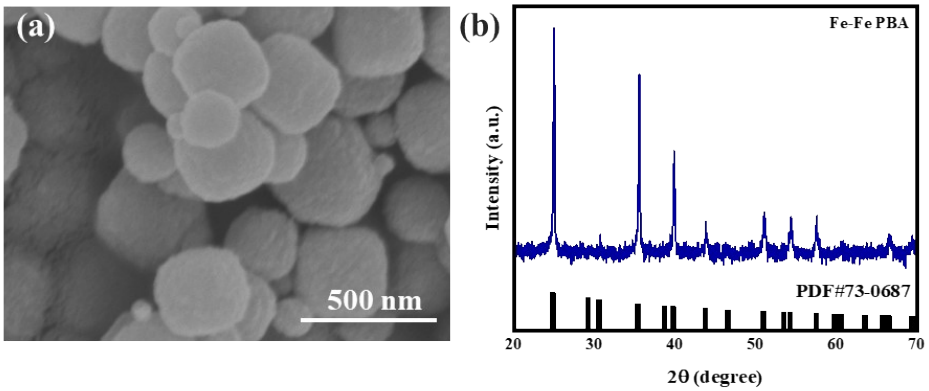

Figure S3 (a) SEM image and (b) Powder XRD pattern of Fe-Fe PBA.

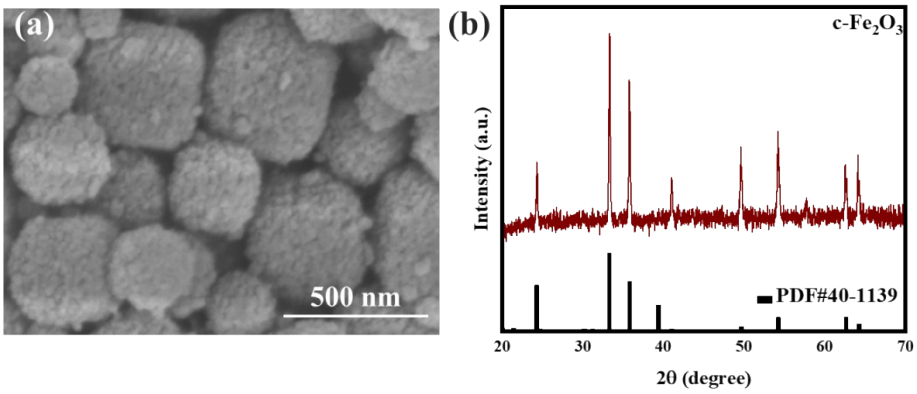

Figure S4 (a) SEM image and (b) Powder XRD pattern of c-Fe_2O_3.

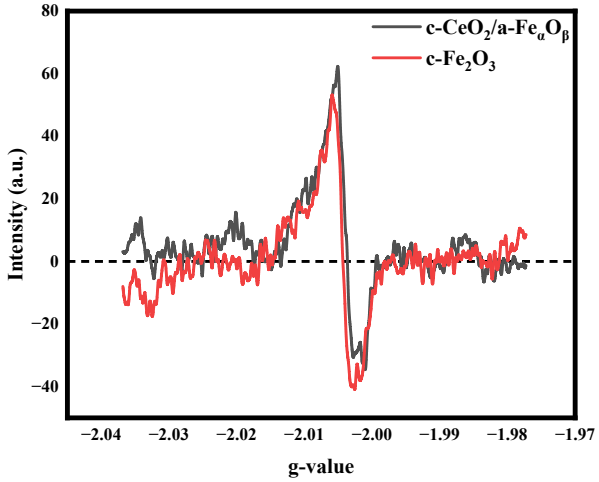

Figure S5 EPR spectra of c-CeO_2/a-$Fe_\alpha O_\beta$ and c-Fe_2O_3.

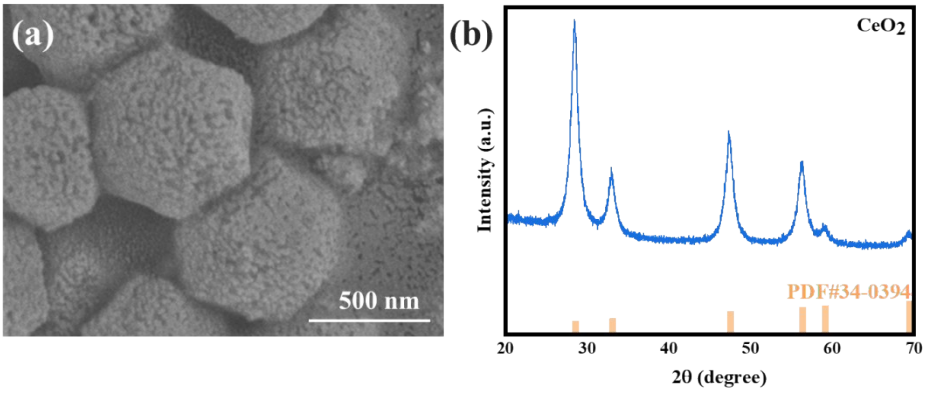

Figure S6 (a) SEM image and (b) Powder XRD pattern of CeO_2.

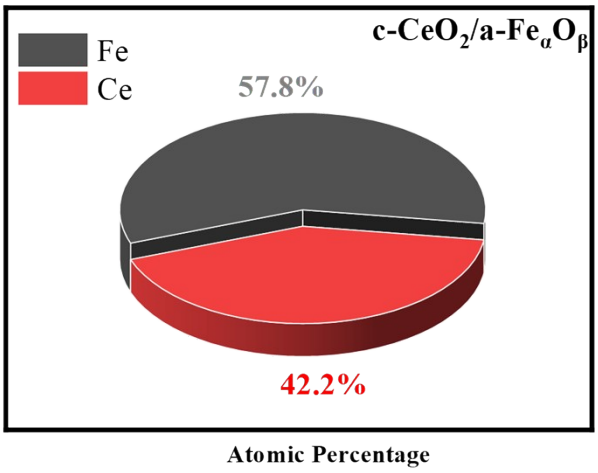

Figure S7 Elemental content detected by ICP testing.

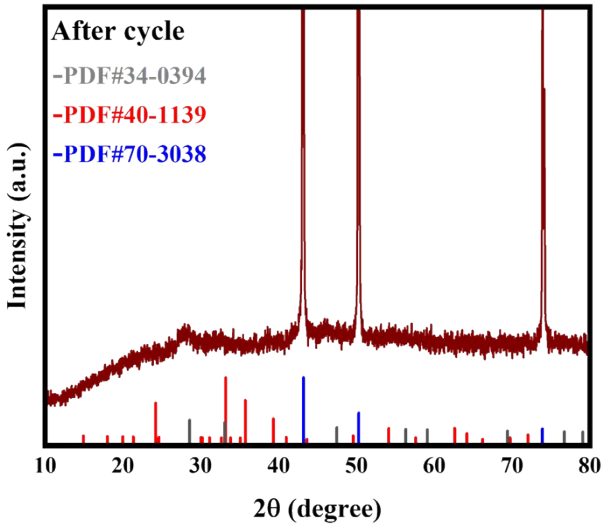

Figure S8 XRD pattern of c-CeO_2/a-$Fe_\alpha O_\beta$ after cycling.

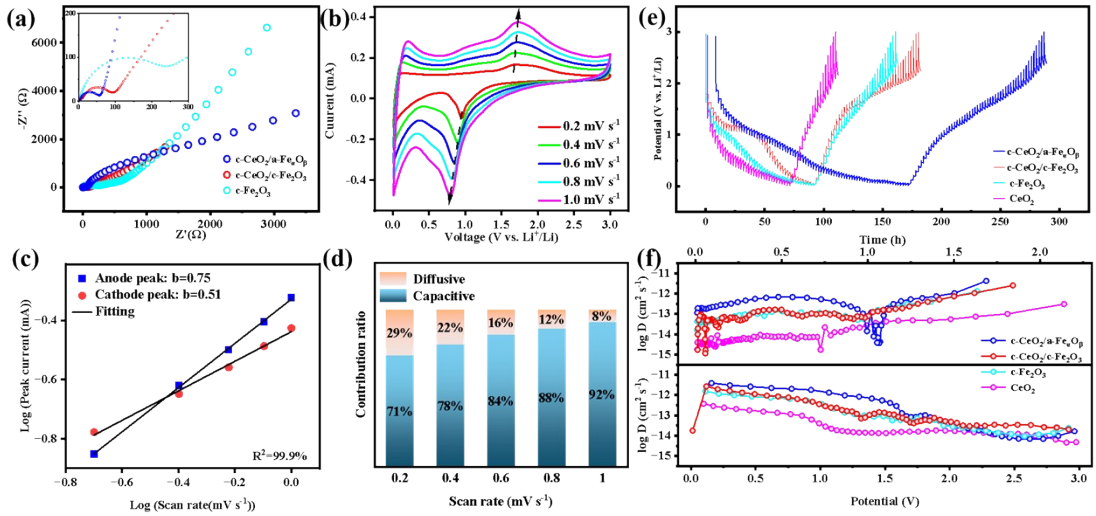

Figure S9 (a) Electrochemical impedance spectra of c-CeO_2/a-$Fe_\alpha O_\beta$, c-CeO_2/c-Fe_2O_3 and c-Fe_2O_3. (b) CV profiles of c-CeO_2/a-$Fe_\alpha O_\beta$ at different scan rates. (c) Slope values of c-CeO_2/a-$Fe_\alpha O_\beta$. (d) Surface capacitive and diffusion contribution at various scan rates of c-CeO_2/a-$Fe_\alpha O_\beta$. (e) GITT profiles and (f) variation of log D with potential for c-CeO_2/a-Fe_2O_3, c-CeO_2/c-Fe_2O_3, c-Fe_2O_3 and CeO_2.

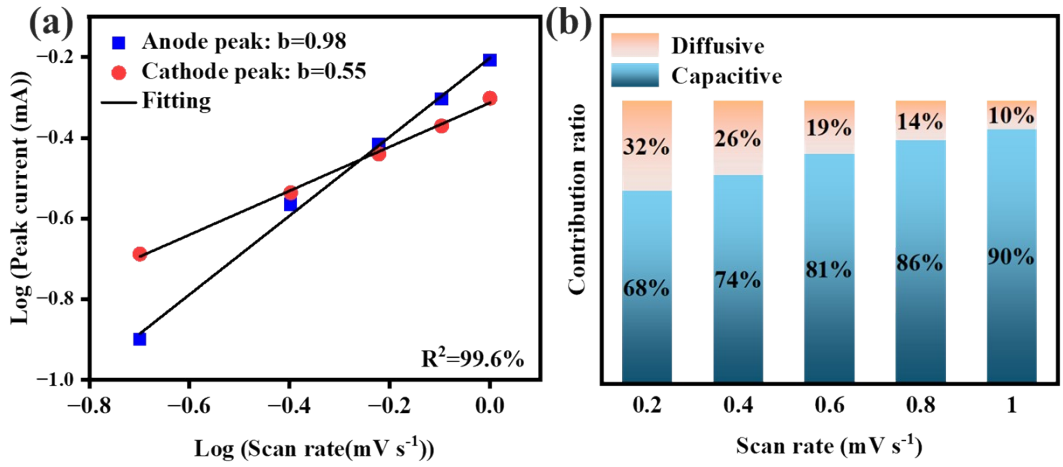

Figure S10 (a) Slope values of c-CeO_2/c-Fe_2O_3 and (b) Surface capacitive and diffusion contribution at various scan rates of c-CeO_2/c-Fe_2O_3.

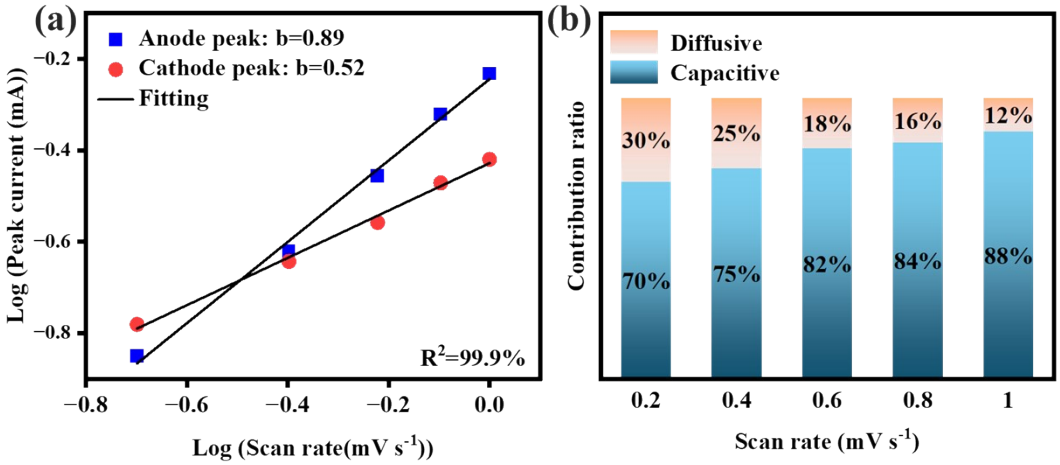

Figure S11 (a) Slope values of c-Fe_2O_3 and (b) Surface capacitive and diffusion contribution at various scan rates of c-Fe_2O_3.